This is the author's accepted manuscript. Posted with permission from the *Annual Review of Marine Science*, Volume 19 © 2027 by Annual Reviews, http://www.annualreviews.org. The version of record is available at https://doi.org/10.1146/annurev-marine-040425-021556.

Turbulence to AMOC: Changes in the North Atlantic

Eleanor Frajka-Williams

Oceanography, Department of Earth System Sciences, University of Hamburg, Hamburg, Germany, 20249; email: eleanor.frajka@uni-hamburg.de
National Oceanography Centre, Southampton, UK, SO14 3ZH

Annu. Rev. Mar. Sci. 2027. 19:1–26

https://doi.org/10.1146/annurev-marine-040425-021556

Copyright © 2027 by the author(s).
All rights reserved

Keywords

meridional overturning circulation, turbulence, AMOC

Abstract

Ocean variability spans a wide range of scales, from centimetres to thousands of kilometres, and seconds to millennia. Turbulence and mixing occupy the smallest scales, with the Atlantic meridional overturning circulation (AMOC) at the largest scales. However, small-scale processes can also affect the large-scale circulation. Past reviews have considered how mixing sets or affects the mean and structure of the Atlantic meridional overturning circulation. In this review, we consider how mixing may affect the time variability of the AMOC. To do this, we first define the AMOC, discuss drivers of variability and how they are manifested in the observed overturning at the RAPID 26°N and OSNAP arrays. We then consider how diabatic processes can change the large-scale overturning circulation.

Contents

1. INTRODUCTION 2
2. CHARACTERISING THE OVERTURNING CIRCULATION 2
   2.1. Quantifying overturning 3
   2.2. Basin-scale geostrophic balance 6
   2.3. Basin-scale thermal wind 6
   2.4. Role of boundary density in overturning 7
3. VARIABILITY OF THE OVERTURNING CIRCULATION 8
4. TURBULENCE AND OVERTURNING 10
   4.1. Water mass transformation 11
   4.2. Deep convection 12
   4.3. Overflows 14
5. LINKING SUBPOLAR CHANGES WITH SUBTROPICAL OVERTURNING 16
   5.1. Propagation of AMOC signals between latitudes 16
   5.2. Boundary vs interior in the subpolar North Atlantic 18
6. DISCUSSION AND OUTLOOK 19

1. INTRODUCTION

The Atlantic Meridional Overturning Circulation (AMOC) transports 10–20 Sv of water across a vast domain, from 35°S to the northern North Atlantic. Besides transporting large volumes of water, it also transports heat northward across all latitudes of the Atlantic, making it a crucial component of the interhemispheric heat budget and a significant moderator of climate across the entire Atlantic basin. The large-scale connectivity of water mass properties across latitudes has invited depictions of the AMOC as a conveyor belt—a slowly varying, laminar system with currents confined to narrow, smooth streams of water (see **Figure 1a**). The real ocean, however, is replete with variability spanning many orders of magnitude in space and time (see **Figure 1b**). This variability is underpinned by turbulent motions—chaotic, multiscale velocity fluctuations—and it poses fundamental challenges for the observation, interpretation, and modelling of the AMOC. Ocean mixing, driven by turbulent processes, maintains abyssal stratification and is a key driver of the global overturning circulation (Munk 1966, Kuhlbrodt et al. 2007), but mixing remains notoriously difficult to parameterise, with different parameterisation schemes producing wide variations in modelled large-scale circulation (Danabasoglu et al. 2014). While there is an extensive literature on closing the time-mean AMOC through tide- and wind-driven mixing, here we focus specifically on the role of turbulent processes—deep convection, overflow entrainment and water mass transformation—in generating both local and remote AMOC variations.

2. CHARACTERISING THE OVERTURNING CIRCULATION

The classic conveyor belt diagram simplifies the four dimensional circulation patterns that make up the AMOC. Despite this limitation, it captures several key characteristics of the circulation: that (i) the AMOC transports water northward in the upper layers of the Atlantic with a southward return flow at depth, (ii) the circulation spans latitudes from the South Atlantic to the North Atlantic, and (iii) sinking in the northern high latitudes

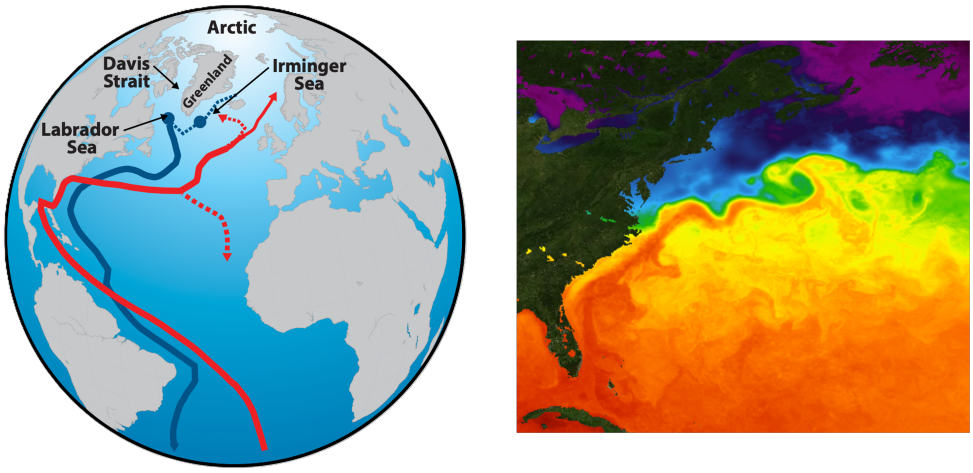


Figure 1

(a) A conveyor belt schematic of the Atlantic meridional overturning circulation showing warm northward currents using red arrows and cold southward currents with blue arrows (Frajka-Williams et al. 2016a). For other variants of the ocean conveyor diagram, see the review in Richardson (2008). (b) A snapshot of sea surface temperature over the Gulf Stream on 22 May 2026 from NASA's GHRSST L4 product (`https://worldview.earthdata.nasa.gov/`), where the region is over the US east coast. Red colors indicate warmer temperatures, while blues and purples represent cooler temperatures.

connects the northward and southward limbs of the circulation. To describe the variability of the overturning and identify how turbulent processes may affect it, we first define the AMOC mathematically, then discuss how changes in the ocean's density structure can give rise to changes in the large-scale circulation. We will see that trans-basin transports are sensitive to changes in the boundary profiles of seawater density—i.e., density variations on the continental slopes—leading to the inference that turbulent processes which affect seawater density at the margins of the Atlantic are able to change the transport strength. This is not to discount the important—possibly dominant—role of adiabatic processes in setting boundary density, but rather to highlight where AMOC transports may be particularly sensitive to diabatic processes.

2.1. Quantifying overturning

To quantify the AMOC, we use the index of the strength of the overturning volume transport given by the overturning streamfunction $\Psi(z)$. Given the meridional velocity field $v(x, z, t)$ at a fixed latitude, the overturning streamfunction in depth space is given by

$$\Psi(y, z, t) = \int_{z_{\mathrm{bot}}(y)}^{z} \int_{x_w(y,z')}^{x_e(y,z')} v(x, y, z', t)\, \mathrm{d}x\, \mathrm{d}z', \qquad 1.$$

where $z_{\mathrm{bot}(y)}$ is the seabed, and $x_w(y, z)$ and $x_e(y, z)$ are the western and eastern boundaries of the basin at latitude y. Since the ocean has sloping sidewalls and the basin geometry varies with latitude, the zonal limits depend on both y and z. The streamfunction Ψ has units of volume transport in Sverdrups (1 Sv $= 10^6$ m^{3}s^{-1}). We will concentrate on the

overturning transport in depth space; however, alternative definitions are also routinely used and have different properties and interpretation (see Sidebar: Density-space overturning). The index for AMOC strength MOC_z is then given by the maximum of the streamfunction, or

$$\mathrm{MOC}_z(y,t) = \max_z \Psi(y,z,t) \ . \qquad 2.$$

Conceptually, the streamfunction is equivalent to taking the zonally averaged vertical profile of north–south velocity at a single latitude, multiplying it by the area of the basin at each depth, and accumulating the result from the seabed upwards. The MOC_z index is then the net northward transport above the depth of maximum overturning $z_{moc}(y,t)$, so that $\mathrm{MOC}_z(y,t) = \Psi(y, z_{moc}, t)$.

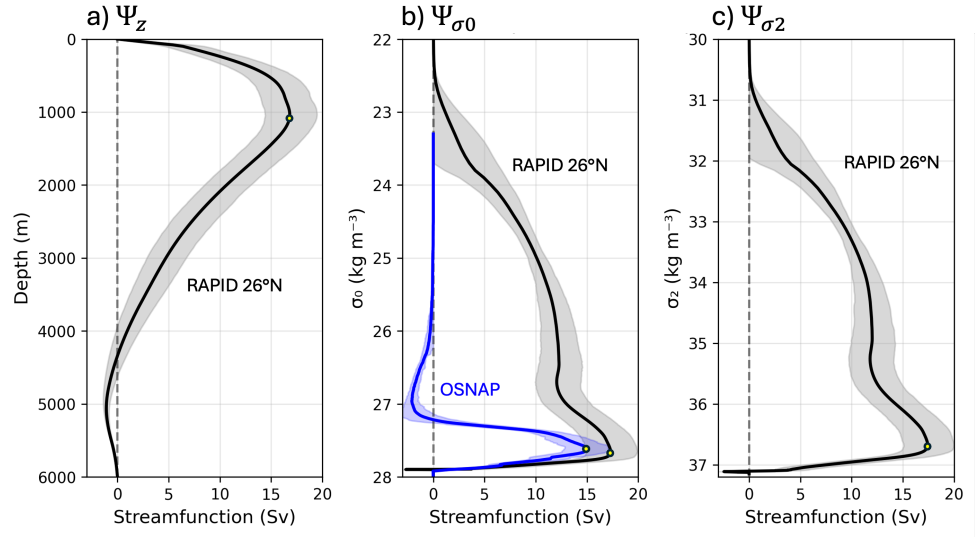


Figure 2

Overturning streamfunction in (a) depth, (b) density σ_0 and (c) density σ_2 space from observations at 26°N (black) and the OSNAP array in the subpolar North Atlantic (blue). The small circles show the value of the maximum of the overturning or MOC_z, $\mathrm{MOC}_{\sigma 0}$ and $\mathrm{MOC}_{\sigma 2}$, respectively. Shading indicates the interquartile range at each depth or density.

Overturning in depth-space closely reflects the terminology of the AMOC itself: a meridional circulation (the vertical integral of meridional velocity) that overturns or reverses direction (change in slope of $\Psi(z)$ as a function of depth). At 26°N, the streamfunction typically exhibits a maximum near 1100 m depth (i.e., $z_{moc} \approx 1100$ m), corresponding to net northward transport above and net southward transport below that depth (see **Figure 2a**). At 26°N in the Atlantic, the southward transport layers are referred to as North Atlantic Deep Water (NADW) with the upper NADW between 1100 and 3000 m, and lower NADW between 3000 and 5000 m. A minimum in the streamfunction at abyssal depths (near 5000 m) represents the lower overturning cell, associated with northward flowing Antarctic Bottom Water which is balanced by a portion of the southward flowing NADW.

We have used, for simplicity, a definition at a fixed latitude where meridional velocities are perpendicular to a zonal section. More generally, the streamfunction can be computed

across any section that spans from coast to coast on the western and eastern boundaries of the Atlantic, using the velocity component perpendicular to that section. For non-zonal sections, the interpretation as a meridional overturning requires care, since the section may span a range of latitudes and potentially crossing between dynamically distinct regions such as the subtropical and subpolar gyres. There is also no requirement for the streamfunction $\Psi(z = 0)$ to vanish; deviations from zero represent a net throughput of water due to e.g., Bering Strait transport from the Pacific to the Atlantic, or volume changes due to riverine input, ice melt or changes in evaporation and precipitation. Observations of the AMOC typically assume no net throughput in order to constrain the velocity field; as a consequence, the streamfunctions in **Figure 2** return to zero at the surface (McCarthy et al. 2015, Frajka-Williams et al. 2019).

2.2. Basin-scale geostrophic balance

While ocean circulation can be observed using current meter measurements, in practice this is impractical at basin scales. Instead, large-scale circulation is determined using geostrophic balance. Meridional geostrophic velocity is related to zonal gradients in pressure as

$$v_g = \frac{1}{\rho_0 f}\frac{\partial p}{\partial x} \ , \qquad 5.$$

where ρ_0 is a constant reference density, f the Coriolis parameter, and p pressure varying in x, z, and t. As we have restricted our discussion to overturning at a single line of latitude, f is constant and drops out of the integral. Over large distances and where we are interested in the net northward flow as for the AMOC, applying geostrophic balance has the advantage that it naturally provides an average of the velocity profile between two longitudes. To apply geostrophic balance instead of using direct current measurements, we assume that ageostrophic flow is relatively small outside of the surface Ekman layer (Sinha et al. 2018). Direct comparisons between thermal-wind-derived velocities and current meter measurements in boundary current regions support this assumption, finding agreement up to a depth-independent (barotropic) offset (Johns et al. 2008). In this simplification, the total meridional velocity used for Equation (1) is $v = v_g + v_{ek}$, where $v_{ek}(z) = -\tau^x/(\rho_0 f D_{ek})$ is a vertical profile of the meridional Ekman velocity given a zonal wind stress τ^x and assuming the transport is uniformly distributed over the Ekman-layer depth D_{ek}. Following Buckley & Marshall (2016), with these simplifications the overturning streamfunction becomes

$$\begin{aligned}\Psi(z,t) &= \Psi_{\mathrm{g}}(z,t) + \Psi_{\mathrm{ek}}(z,t) \\ &= \int_{z_{\mathrm{bot}}}^{z} \frac{p_e(\tilde{z},t) - p_w(\tilde{z},t)}{\rho_0 f}\,\mathrm{d}\tilde{z} + \int_{z_{\mathrm{bot}}}^{z}\int_{x_w}^{x_e} v_{\mathrm{ek}}\,\mathrm{d}x\,\mathrm{d}z \ , \end{aligned} \qquad 6.$$

where p_e and p_w are the ocean pressures at x_e and x_w, the eastern and western boundaries of the basin, respectively. The subscript $\cdot_g$ denotes the geostrophic contribution to the streamfunction (Hughes et al. 2013).

While the Ekman component of meridional velocity contributes to overturning strength and variability, the Ekman component tends to be more important on annual and shorter timescales; the geostrophic component carries more of the variance on interannual and decadal timescales (Moat et al. 2020). In a numerical model, Hughes et al. (2018) demonstrated that the seabed pressure anomalies at the boundaries of the Atlantic capture a majority of the variability of the AMOC. In the remainder of this paper, we focus primarily on the geostrophic component of overturning.

Sidebar: Density-space overturning

Overturning in density space can better capture some aspects of overturning structure than depth space, including clearer separation between overturning cells across the subtropics, subpolar North Atlantic and Nordic Seas, and the density of maximum overturning (σ_{moc}). It is also more directly linked to water mass transformation processes, since changes in the density-space streamfunction reflect convergence and divergence of cross-isopycnal transport, which is set by surface buoyancy forcing and interior diapycnal mixing (Groeskamp et al. 2018). The differences between density- and depth-space streamfunctions can themselves be physically informative: in the subpolar gyre, the discrepancy has been interpreted as evidence for horizontal circulation across sloping isopycnals (Zhang & Thomas 2021), while at 26.5°N it reveals a shallow subtropical overturning cell associated with subtropical mode water formation that is partly cancelled in depth-space accumulation (Tooth et al. 2024). For a discussion of the merits of the density-space definition, see Foukal & Chafik (2024); Danabasoglu et al. (2025) further recommend using both density and depth space definitions simultaneously since they provide complementary information.

As a concrete example, in the subpolar North Atlantic the northward transport of relatively warm waters occurs primarily in the upper ocean of the eastern basin, while southward transport of colder waters is concentrated along the western boundaries across a broad depth range—a pattern more readily captured in density coordinates than at fixed depths (Lherminier et al. 2007, Foukal & Chafik 2024). The density-space overturning streamfunction $\Psi(\sigma, t)$ is then

$$\Psi(y, \tilde{\sigma}, t) = \int_{x_w(y)}^{x_e(y)} \int_{z_{\mathrm{bot}}(y)}^{z_{\mathrm{surf}}} v(x, y, z, t)\, H(\sigma(x, y, z, t) - \tilde{\sigma})\; dz\, dx, \tag{3.}$$

where H is the Heaviside function, equal to 1 where $\sigma(x, y, z, t) > \tilde{\sigma}$, i.e. where the local potential density anomaly exceeds the specified density class, and 0 otherwise. For non-zonal sections, this expression generalizes by replacing the integration along x at fixed y with integration along the section, using the velocity component normal to it. In this formulation, $\Psi(\sigma, t)$ represents the cumulative meridional transport of water denser than σ rather than the transport of water below a depth level (see **Figure 2b,c**). This definition avoids the need to explicitly transform the governing equations into density coordinates.

The overturning strength in density space is defined by

$$\mathrm{MOC}_\sigma(y, t) = \max_{\sigma} \Psi(y, \sigma, t)\ . \tag{4.}$$

The choice of density variable for the overturning coordinate varies, with some groups using σ_0 (Lozier et al. 2019), σ_2 (Moat et al. 2026) or neutral density γ_n (Fox et al. 2026). There is no consensus on which choice is most appropriate, but the choice does affect the magnitude and variability of overturning, as well as details of its interpretation (Danabasoglu et al. 2025).

2.3. Basin-scale thermal wind

Most AMOC observing systems estimate geostrophic currents using the thermal wind relation (Frajka-Williams et al. 2019). Thermal wind relates the vertical shear in meridional velocity to the zonal gradient in seawater density as

$$\frac{\partial v_g}{\partial z} = -\frac{g}{\rho_0 f}\frac{\partial \rho}{\partial x}\ , \tag{7.}$$

where g is gravitational acceleration and ρ is seawater density. Density, derived from *in situ* measurements of temperature and salinity, can then be used to estimate velocity (Frajka-Williams et al. 2019, 2023). While the use of density instead of pressure has observational advantages, it requires knowledge of a reference velocity, since thermal wind yields only the vertical shear. To go from $\partial v_g/\partial z$ to v_g, we require a constant of integration termed the level of known motion (v_{ref}) or level of no motion ($v_{ref} = 0$).

Applying thermal wind, we can write the overturning streamfunction following Marotzke et al. (1999) and Buckley & Marshall (2016) as

$$\Psi(z,t) = \underbrace{\frac{g}{\rho_0 f}\int_z^0 \int_{z_{\rm bot}}^{z'} \big(\rho_w(\tilde{z},t) - \rho_e(\tilde{z},t)\big)\,\mathrm{d}\tilde{z}\,\mathrm{d}z'}_{\Psi_{\rm tw}(z,t)} + \underbrace{A(z)\overline{v}_{\rm ref}(t)}_{\Psi_{\rm ext}(z,t)} + \Psi_{ek}(z,t) \qquad 8.$$

where $A(z) = \int_z^0 \int_{x_w}^{x_e} dx\,dz$ is the cross-sectional area of the basin from depth z to the surface, and $\overline{v}_{\rm ref}(t)$ is a depth-independent velocity. Physically, $\overline{v}_{\rm ref}$ corresponds to the zonal average of the reference velocity, which is in geostrophic balance with horizontal pressure gradients rather than density gradients, and therefore is not constrained by thermal wind. In this formulation, Ψ_{tw} is the thermal wind component of overturning and Ψ_{ext} the external or compensation component.

The depth-independent (barotropic) component of the flow is a real feature of the circulation, and its time-varying part can in principle be inferred from differences in ocean bottom pressure across the basin (Kanzow et al. 2007, Worthington et al. 2019). However, the absolute accuracy and long-term stability of *in situ* bottom pressure measurements currently limit the use of this approach for monitoring the AMOC over long timescales (Hughes et al. 2018). As a result, overturning arrays do not directly measure $\overline{v}_{\rm ref}$ (neither the time-mean nor the time-varying reference level velocity) and instead apply a compensation velocity chosen to enforce a closure constraint on the streamfunction (Frajka-Williams et al. 2019). The RAPID-MOCHA-WBTS (RAPID-Meridional Overturning Circulation and Heat transport Array-Western Boundary Time Series) array at 26°N (hereafter, RAPID 26°N) chooses a $\overline{v}_{\rm ref}$ at each time step to ensure the streamfunction $\Psi(z,t)$ vanishes at the surface (see **Figure 2a**). The OSNAP array (Overturning in the Subpolar North Atlantic Program) first references velocities to time-mean altimetric velocity field and then applies a compensation velocity so that the streamfunction $\Psi(\sigma,t)$ starts and ends at zero (see **Figure 2b**; Li et al. 2017). The treatment of the compensation introduces ambiguity into estimates of overturning from observing arrays since the depth-independent component of the transbasin transport is not directly observed (see Frajka-Williams et al. 2023, for a discussion).

2.4. Role of boundary density in overturning

Applying the no-net-flow closure to $\overline{v}_{\rm ref}$ in eq. (8), the geostrophic-shear component of MOC_z—i.e. thermal wind plus barotropic compensation, excluding Ekman—reduces to a single weighted integral of the trans-basin density difference (Waldman et al. 2021, eq. 14):

$$\begin{aligned}\mathrm{MOC}_z^{g\text{-}sh}(t) \approx \frac{g}{\rho_0 f}\Bigg[&(-z_{moc})\int_{z_{\rm bot}}^{z_{moc}} \left(1+\frac{\tilde{z}}{h}\right)\big(\rho_w(\tilde{z},t)-\rho_e(\tilde{z},t)\big)\,\mathrm{d}\tilde{z} \\ &+\left(1+\frac{z_{moc}}{h}\right)\int_{z_{moc}}^{0}(-\tilde{z})\big(\rho_w(\tilde{z},t)-\rho_e(\tilde{z},t)\big)\,\mathrm{d}\tilde{z}\Bigg],\end{aligned} \qquad 9.$$

where $h = -z_{\mathrm{bot}}$ is the basin depth. (Waldman et al. 2021 denote this $\mathrm{AMOC}_{g\text{-}sh}$ and write the density difference with $\Delta\rho = \rho_e - \rho_w$, the opposite sign convention from ours.) The Ekman contribution under the same no-net-flow closure is $(1 + z_{moc}/h)\,\mathrm{MOC}_z^{\mathrm{ek}}$ (Waldman et al. 2021, eq. 13), so that $\mathrm{MOC}_z = \mathrm{MOC}_z^{g\text{-}sh} + (1 + z_{moc}/h)\,\mathrm{MOC}_z^{\mathrm{ek}}$.

The weight on $(\rho_w - \rho_e)$ is triangular: it vanishes at both the seabed and the surface and peaks at z_{moc} with value $|z_{moc}|(1 + z_{moc}/h)$. Density anomalies near z_{moc} therefore exert the strongest leverage on MOC_z, whether they arise from adiabatic processes (such as boundary isopycnal displacement) or from diabatic processes (such as deep convection, mixing, or surface buoyancy fluxes that modify the density of newly formed water masses). The weight is a sensitivity rather than a contribution, however: the depths that dominate MOC_z variability are set by its product with the amplitude of $(\rho_w - \rho_e)$ variability, which is itself generally larger in the upper ocean and need not peak at z_{moc}.

To make this concrete, a lightening of Labrador Sea Water at the western boundary—whether by diabatic processes such as deep convection or by adiabatic transport from upstream—reduces $\rho_w - \rho_e$ near z_{moc} and so reduces $\mathrm{MOC}_z^{g\text{-}sh}$ (see Polo et al. 2014, and references therein). The remainder of the paper examines the turbulent processes that modify boundary density and, through the weighting in eq. (9), the overturning.

3. VARIABILITY OF THE OVERTURNING CIRCULATION

The drivers of AMOC variability span a wide range of processes and timescales (see **Figure 3**). These include the direct effect of surface Ekman transport due to zonal winds, water mass transformation through heat loss in the northern high latitudes, contributions from overflows supplying dense water from the Nordic Seas, and planetary and boundary wave adjustment processes. In the Southern Ocean, wind-driven upwelling sustains the southward return flow of NADW by drawing it upwards along isopycnals. For a detailed review of AMOC drivers, see Buckley & Marshall (2016).

The boundary density framework developed in the previous section (Equation 8) provides a useful organising principle: to affect the thermal wind-driven component of overturning strength, a process must modify the zonal density gradient at the boundaries of the Atlantic. These modifications can arise through two broad classes of processes. *Adiabatic* processes—including wind-forced Rossby wave adjustment, wind-forced isopycnal heave, and barotropic pressure changes—redistribute existing density surfaces without modifying water mass properties, and can communicate changes rapidly across the basin. *Diabatic* processes—including deep convection, entrainment of the overflows from the Nordic Seas, and water mass transformation due to heat loss in the northern high latitudes—result in irreversible modifications to water mass properties.

Theory and numerical models indicate that large-scale circulation changes can propagate rapidly along boundaries and across basins through adiabatic dynamical adjustment (see Johnson et al. 2019, and references therein). These adjustment timescales—typically 1–10 years in models—are much shorter than Lagrangian estimates of water mass transit times for water parcels travelling from the subpolar to subtropical North Atlantic, which can exceed two decades (Zou & Lozier 2016). This distinction suggests that wave-mediated adjustment of the AMOC to subpolar forcing occurs on timescales of years rather than decades.

Changes in boundary density—whether driven by adiabatically displaced isopycnals or by diabatically modified water mass properties—determine overturning strength at sub-

tropical and mid-latitudes, where the thermal wind framework applies most cleanly.

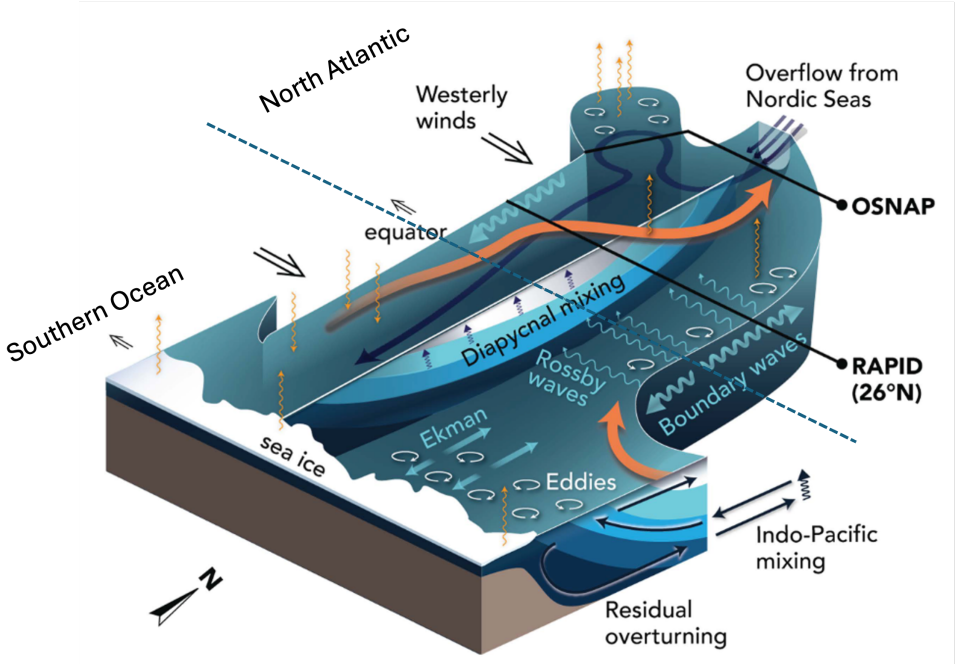


Figure 3

Schematic of the key processes which affect the AMOC, as well as the locations of monitoring arrays in the North Atlantic (RAPID at 26.5°N and OSNAP in the subpolar North Atlantic). The lower left of the figure represents Antarctica, and the upper right the northern North Atlantic. Reproduced from Johnson et al. (2019).

To date, the variability of the overturning at 26°N has mostly been explained by adiabatic processes. The AMOC at 26°N has been observed using a moored array since 2004 (see **Figure 4**; Moat et al. 2026). Overturning variability is dominated by wind forcing (Jackson et al. 2022, and references therein). The seasonal variability is explained by wind stress curl at the eastern boundary near the Canary Islands which drives vertical displacements of isopycnals at the eastern boundary (depressed in autumn, shoaled in spring) and produces a seasonal AMOC cycle with a maximum in October and a minimum in April (Kanzow et al. 2010, Chidichimo et al. 2010, Duchez et al. 2014a). Using a simple two-layer model, Zhao & Johns (2014a) show more broadly that, across the subtropical and mid-latitude North Atlantic, the seasonal cycle of the AMOC is dominated by changes at the eastern boundary; in the South Atlantic, both western and eastern boundaries contribute.

On interannual timescales, contributions from the western boundary dominate over the eastern boundary (Polo et al. 2014, Frajka-Williams 2015). Variations, including the persistent dip in 2009/10, can also be explained by wind forcing (Evans et al. 2017) where both meridional Ekman and geostrophic transport changes contribute (McCarthy et al. 2012). The geostrophic changes result from adjustment via westward propagating planetary waves (Zhao & Johns 2014b) associated with a deepening of the thermocline at the western boundary (Frajka-Williams et al. 2016b). The relatively strong AMOC in 2005 can also

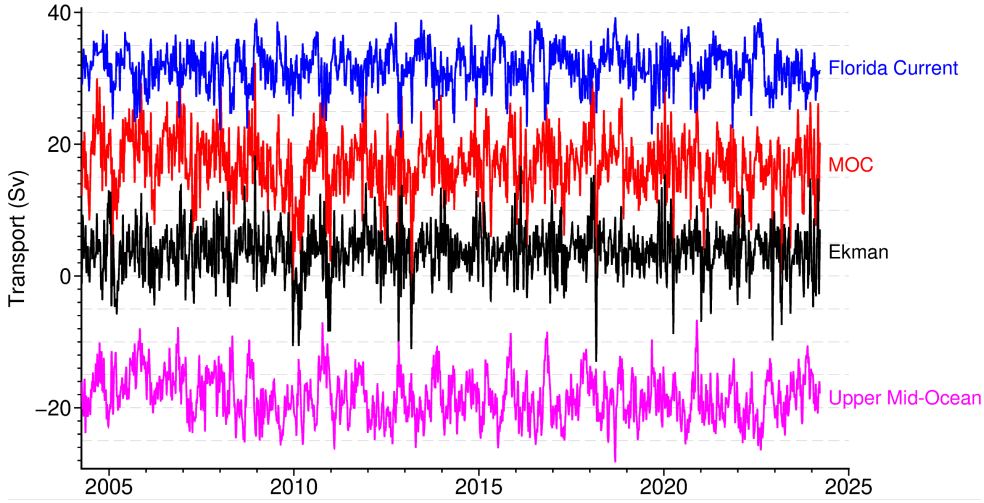


Figure 4

Time series of overturning strength at 26°N (red) and its components: the Gulf Stream transport through Florida Straits (blue), Ekman transport applied in the upper 100 m (black) and the upper mid-ocean transport which is the net transport in the upper roughly 1100 m due to (i) thermal wind, (ii) the compensation transport and (iii) the current meter measurements in the western 25–45 km of the basin. Data are from the RAPID 26°N array (Moat et al. 2026).

be explained by adjustment to wind forcing with an associated uplifted thermocline at the western boundary (Zhao & Johns 2014b). A numerical model study found that the AMOC at 26°N adjusts to wind forcing within 2–3 years (Duchez et al. 2014b). This is shorter than the time it would take for a Rossby wave to cross the 6000 km basin at 26.5°N at a speed of 4–5 cm s^{-1}. Idealised modelling studies suggest that in an ocean with a mid-basin ridge, the adjustment to wind anomalies east of the ridge first occurs as a barotropic signal; upon encountering the ridge, the barotropic anomaly sheds baroclinic waves that propagate westward to the boundary (Andres et al. 2012). The result is that the baroclinic wave adjustment only needs to span the 2700 km from the mid-Atlantic ridge at 50°W to the boundary at 77°W to affect overturning. Both the seasonal and interannual variability of the AMOC at 26°N can be explained by adiabatic processes. On longer timescales, new evidence suggests that both the eastern and western boundaries contribute to AMOC variability (Xing et al. 2026).

At 26°N on these timescales, adiabatic adjustment to wind forcing therefore dominates the observed variability. This is not the full story for the AMOC: the dense water masses that fill the lower limb must be created somewhere, by diabatic processes; once formed, their properties propagate equatorward (Johnson & Marshall 2002) and set the long-timescale envelope on which the wind-driven variability at 26°N rides (Buckley & Marshall 2016, Yeager et al. 2021). The remainder of this paper examines those turbulent processes—deep convection, overflow entrainment, and boundary mixing—and the pathways by which they reach the subtropical AMOC.

4. TURBULENCE AND OVERTURNING

For the steady-state overturning, the dense water formed at high latitudes must return to the surface somewhere. Diapycnal mixing across the basin interior supplies at least part of this return upwelling (Cimoli et al. 2023), with adiabatic wind-induced upwelling in the Southern Ocean supplying another portion (see review by Kuhlbrodt et al. 2007, and references therein). Recent advances have refined this picture, identifying that the intensification of mixing near the seabed and basin geometry together confine abyssal upwelling to narrow regions near the boundaries (see Johnson et al. 2019, and references therein). Whether interior mixing plays a significant role in the overturning, or whether the circulation is primarily adiabatic, remains an open question. de Lavergne et al. (2021) provide an overview of how mixing shapes the large-scale mean circulation and overturning through three principal effects: (1) modifying surface wind and buoyancy forcing, (2) producing and consuming water masses, and (3) altering density gradients. In what follows, we focus on the second and third of these effects as they relate to AMOC variability. Specifically, we consider water mass transformation across the subpolar gyre in §4.1, with particular attention to deep convection in §4.2, and dense water overflows in §4.3. In §5, we examine how these diabatic processes contribute to AMOC variability at lower latitudes through adiabatic mechanisms.

4.1. Water mass transformation

The overturning streamfunction in density space $\Psi(\sigma, t)$ (Equation 3) provides a natural framework for understanding how turbulent processes drive AMOC variability. It is especially relevant in the subpolar North Atlantic where steeply sloping isopycnals mean that depth and density coordinates capture very different aspects of the flow (Lherminier et al. 2007, Desbruyères et al. 2019, Zhang & Thomas 2021, Danabasoglu et al. 2025). Unlike $\Psi(z, t)$, which captures the depth-space structure of meridional transport, $\Psi(\sigma, t)$ directly relates to the rate at which water masses are transformed across density surfaces. The subpolar overturning as measured at OSNAP, which spans from Labrador to Greenland to Scotland, is fundamentally diabatic: it represents the transformation of warm, light Atlantic Water into cold, dense NADW north of the array.

The water mass transformation (WMT) framework, formalised by Walin (1982) and reviewed in Groeskamp et al. (2018), links the strength of the overturning in density space to its diabatic drivers. In the absence of diapycnal mixing, cross-isopycnal volume fluxes at any latitude must be accounted for entirely by air–sea buoyancy fluxes at the outcrop of the relevant density surface: water densified by buoyancy loss in one region must be balanced by lightening transformations elsewhere, so that the net surface-forced transformation across each isopycnal outcrop sets the overturning strength at that density class. When diapycnal mixing is also present, surface forcing no longer accounts for the full cross-isopycnal flux; in steady state, the framework allows the interior transformation to be inferred from the surface forcing by requiring net fluxes to balance for each density class, while in transient states an imbalance instead appears as a tendency in the volume of the corresponding water mass class. Because surface buoyancy fluxes are more directly tied to the diabatic drivers of the circulation than velocity-based transport estimates, the WMT framework provides both a diagnostic and a predictive tool for understanding the mean overturning and its variability.

4.1.1. Role in mean AMOC. Applying the WMT framework in the subpolar North Atlantic demonstrates that air–sea buoyancy fluxes alone cannot account for the magnitude of overturning at OSNAP; a residual mixing-driven transformation is also required (Evans et al. 2023). Cooling by air–sea heat fluxes and mixing-driven freshening in the Nordic Seas, Iceland Basin and Irminger Sea transform the warm, salty Atlantic Water to subpolar mode water classes. Mixing in the interior of the Nordic Seas, over the Greenland–Scotland Ridge, and along the boundaries of the Irminger Sea and Iceland Basin then drives the accumulation of water in the density classes associated with NADW. Air–sea buoyancy fluxes and mixing therefore play distinct but complementary roles in setting the time-mean subpolar overturning strength (Evans et al. 2023).

4.1.2. Role in AMOC variability. The surface-forced component of the WMT framework may also provide predictive skill for decadal AMOC variability. Desbruyères et al. (2019) showed that anomalies in the rate of warm-to-cold water mass transformation at high latitudes precede overturning changes at 45°N by 5–6 years, capturing the 1993–2010 decline in overturning and subsequent recovery. This lagged relationship arises because surface-forced density anomalies must be exported from the subpolar gyre into the boundary current system and advected equatorward before they influence overturning at mid-latitudes—the same propagation pathway that links Labrador Sea density anomalies to subtropical overturning changes (Böning et al. 2006). The WMT framework thus provides a direct link between subpolar water mass transformation, decadal AMOC variability and North Atlantic ocean heat content changes.

4.2. Deep convection

In the wintertime northern North Atlantic, intense heat loss from the ocean to the atmosphere combines with weakened stratification to drive deep convection. Surface waters become denser than those beneath, creating gravitational instability that triggers convective plumes penetrating downward with instantaneous vertical velocities w exceeding 10 cm s^{-1} (Marshall & Schott 1999, Steffen & D'Asaro 2002, Frajka-Williams et al. 2011). These plumes generate vigorous three-dimensional turbulence that efficiently homogenizes temperature and salinity within the convective chimney over the upper 500–2000 m of the water column (Clément et al. 2024). After formation, restratification caps the convection, leaving behind a relatively homogeneous water mass that then circulates within the interior Labrador and Irminger Seas or is exported southward in the boundary current (Li & Lozier 2018). While convection is often conflated with the net sinking required to close the overturning (Kuhlbrodt et al. 2007), it contributes very little to net sinking. (Note that convection, deep water formation and sinking are often used interchangeably; see the Sidebar: Convection, Deep Water Formation, and Sinking for an explanation of how these terms are used.) Although the vertical seawater velocity w is large and downward within convective plumes, compensating upwelling occurs between them, so the net vertical transport is small. As a result, Labrador Sea convection accounts for only ∼2 Sv compared with an overturning strength of ∼17 Sv (Pickart & Spall 2007), and the closure of the deep limb's return flow must happen elsewhere. Its contribution to the density of newly formed deep water, and the consequences for mean NADW properties and AMOC variability, are examined in turn.

4.2.1. Role in mean NADW properties. Deep convection modifies the properties of Labrador Sea Water (LSW), the upper layer of NADW. Models tend to overestimate the depth of convection and overproduce LSW relative to observations (Li et al. 2019, Heuzé 2021), and this bias affects the simulated density structure of the deep western boundary current (DWBC) and the mean AMOC. Proxies commonly used to infer Labrador Sea convection intensity—such as the wintertime maximum mixed layer depth—do not reliably represent the overturning in the Labrador Sea (Li & Lozier 2018). Small-scale turbulent processes active during deep convection, including the lateral flux of freshwater from the surrounding stratified waters into the convective region (Schiller-Weiss et al. 2024, Clément et al. 2023), may further limit the depth and density of convective products, and remain poorly represented in climate models (Heuzé 2021).

4.2.2. Role in AMOC variability. The relationship between Labrador Sea convection and AMOC variability has been substantially revised in light of observational and modelling evidence. Modelling studies established a close correspondence between convection intensity and deep western boundary current transport, with convection leading AMOC changes at subtropical latitudes by 1–2 years via the southward advection of density anomalies to 45°N followed by rapid wave adjustment processes (Zhang et al. 2019). Density anomalies in the 1000–2500 m Labrador Sea layer were also shown to lead overturning changes at 26.5°N (see **Figure 5a** and Robson et al. 2014, Jackson et al. 2016). However, Lozier (2012) found insufficient observational evidence for a direct link between subpolar convection and DWBC variability; the OSNAP array provided observational evidence that subpolar overturning is dominated by water mass transformation east of Greenland rather than in the Labrador Sea (Lozier et al. 2019). An independent estimate using the WMT framework reached the same conclusion (Desbruyères et al. 2019). Moreover, the region of maximum transformation is east of the Reykjanes Ridge, so that neither convection in the Labrador Sea nor the Irminger Sea is implicated (see **Figure 5b**).

Part of the discrepancy between models and observations reflects the model biases described above. A multimodel analysis found that while all models display a strong local relationship between LSW volume and overturning in the Labrador Sea, the relationship degrades considerably downstream with no consistent signal at subtropical latitudes on interannual to decadal timescales (Li et al. 2019). The apparent contradiction is partly resolved by considering timescale and forcing amplitude. Under normal interannual variability, Labrador Sea convection has negligible impact on AMOC—consistent with OSNAP—but under exceptional forcing the impact can be substantial: the anomalously cold winters of the early 1990s may have induced an AMOC anomaly exceeding 20%, driven by the rapid spreading of mid-depth density anomalies from the Labrador Sea into the Irminger Sea (Böning et al. 2023). Notably, the Labrador–Irminger density coupling appears bidirectional: Menary et al. (2020) found that density anomalies generated in the Irminger Sea can propagate into the Labrador Sea and dominate its density variability, suggesting that correlations between Labrador Sea density and AMOC strength may sometimes reflect Irminger Sea forcing rather than a direct causal influence of Labrador Sea convection. On multidecadal timescales, an eddy-resolving simulation nonetheless finds that sustained anomalous LSW production plays a substantial role in AMOC variability (Yeager et al. 2021), and observation-based estimates suggest a relationship between Labrador Sea convection and subpolar overturning on pentadal and longer timescales (Fox et al. 2026). The OSNAP observational record of subpolar overturning is not yet long enough to test whether

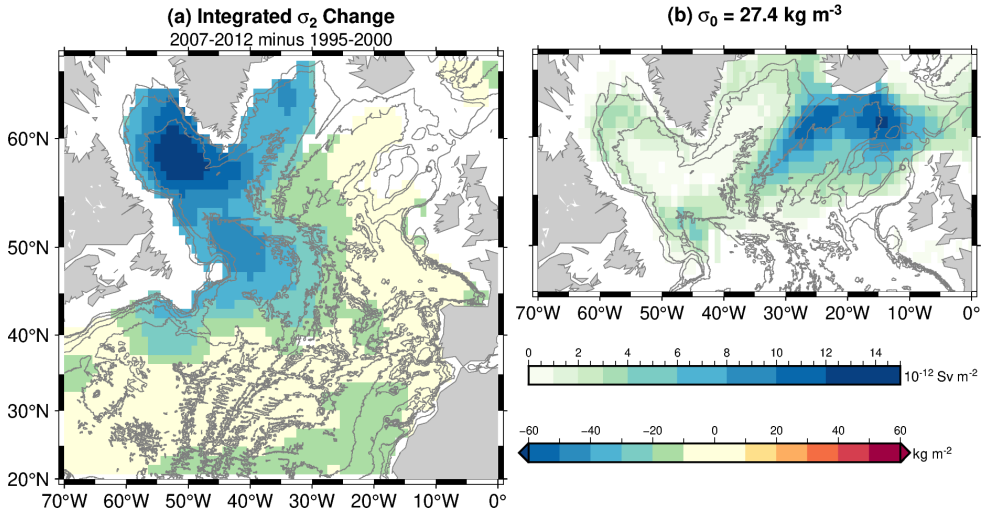


Figure 5

Subpolar changes and the AMOC showing (a) the difference in σ_2 density as the 2007–2012 average minus the 1995–2000 average of density integrated from 1000–2500 m. Following Robson et al. (2014), but using the EN4 dataset (Good et al. 2013), and (b) the time-mean surface-forced transformation across the isopycnal surface $\sigma_0 = 27.4$ kg m^{-3} in units of Sv m^{-2} for 1993–2017 (plotted using data from Buckley et al. 2023 provided by D. Desbruyères, pers. comm.). EN.4.2.2 data were obtained from `https://www.metoffice.gov.uk/hadobs/en4/` and are © British Crown Copyright, Met Office, [last access: June 17, 2025], provided under a Non-Commercial Government Licence (`http://www.nationalarchives.gov.uk/doc/non-commercial-government-licence/version/2/`).

convection affects low frequency, subpolar AMOC variability. These findings are consistent with the boundary-density framework in §2.4: at 26°N, LSW spans depths of roughly 1000–2400 m, sitting just below z_{moc} (∼1100 m) in the depth range where the weighting in equation (9) remains close to its peak, so density changes in LSW exert stronger leverage on $\mathrm{MOC}_z^{g\text{-}sh}$ than anomalies of comparable magnitude near the surface or seabed.

4.3. Overflows

Overflows of dense Nordic Seas water across the Greenland–Scotland Ridge (GSR) also form NADW, primarily filling the lower layers of the DWBC (Dickson & Brown 1994). Specifically, overflows refer to the cascade of dense waters across relatively shallow sills (e.g., Denmark Strait and the Faroe Bank Channel). Unlike deep convection, overflows contribute directly to net sinking (Hughes & Griffiths 2006, Legg et al. 2009). The two principal overflows—across Denmark Strait and the Faroe Bank Channel—together contribute around 5 Sv to the DWBC (Østerhus et al. 2019). The overflows undergo intense diapycnal mixing immediately downstream of the sills (within ∼200 km for Denmark Strait; Voet & Quadfasel 2010), beyond which entrainment decreases substantially (Price & Baringer 1994). The mixing is primarily caused by shear-driven instabilities at the interface between the dense gravity current and the overlying ambient water, where the Richardson number falls below its critical value of 1/4 (Baringer & Price 1997, Voet & Quadfasel 2010). Bottom

Sidebar: Convection, Deep Water Formation, and Sinking

The terms convection, deep water formation, and sinking are often used interchangeably when discussing the AMOC, but they describe distinct physical processes.

Convection refers to vertical mixing driven by buoyancy loss at the ocean surface, typically observed or quantified by the depth of the winter mixed layer. Convection vigorously redistributes properties within the mixed layer, but produces negligible *net* vertical transport of water. It is a local mixing process that does not directly drive net sinking.

Deep water formation refers to the production of a substantial volume of near-homogeneous deep water through buoyancy loss and mixing. It is a specific case of water-mass transformation, which more generally describes any cross-isopycnal flux and is rigorously defined and quantified in Sverdrups (Sv) using the Walin framework.

Sinking, in the context of the overturning circulation, refers to the net downward transport of water that converts upper-limb flow into the deep return flow. It can occur through subduction along sloping density surfaces, overflow across sills, or gradual descent along boundary currents, and does not require deep convective mixing.

Deep convection, deep water formation, and sinking can occur in the same regions but are not equivalent and should not be used interchangeably when interpreting AMOC variability. Convection is often integral to buoyancy-forced WMT and the two are commonly co-located, but the relationship is not strict: strong convection in weakly stratified water may produce little net WMT, while strong WMT can occur without deep convection—as in the eastern subpolar North Atlantic (**Figure 5b**), where wintertime mixed layers may not exceed 400 m yet transformation rates are large in part because warm, low-density Atlantic Water is being transformed across many density classes. In the depth-space streamfunction $\Psi(y, z)$, the implied downward motion at high latitudes is the sinking; in the density-space streamfunction $\Psi(y, \sigma)$, the cross-isopycnal flux at high latitudes is the deep water formation. The overturning strength in each framework reflects different aspects of the same circulation.

drag and flow over rough topography provide additional turbulence, driving homogenisation of the bottom boundary layer and entrainment of ambient water from above. This entrainment substantially increases the volume of overflow water while reducing its density. Importantly, the final density of the resulting water mass depends only weakly on the density of the source water over the sill, because increasing the density contrast between the overflow and ambient water intensifies the mixing; the volume, in contrast, depends strongly on the density difference, since a larger contrast drives more vigorous entrainment of ambient water (Legg et al. 2006, Danabasoglu et al. 2010).

4.3.1. Role in mean NADW properties. The overflow-entrainment process—operating on dense source waters supplied by the Nordic Seas—is a primary determinant of the density and depth of the lower limb of the AMOC (Danabasoglu et al. 2010). Spurious numerical mixing in depth-coordinate models is often larger than the vigorous physical mixing that should occur (Legg et al. 2006), and the diapycnal mixing downstream of overflow sills directly affects the structure and magnitude of the AMOC (Wang et al. 2015). Including overflow parameterisations improves the North Atlantic mean state considerably, deepening the DWBC and improving tracer distributions, but may also damp AMOC variability by

enhancing Labrador Sea stratification (Yeager & Danabasoglu 2012). Even with the best parameterisation, however, correctly capturing overflows requires both an adequate supply of dense source waters and realistic interior properties for entrainment to act on; biases in surface fluxes or in the upstream water-mass structure therefore limit model fidelity (Danabasoglu et al. 2010). Improving overflow representation in models has been a persistent focus of research (Legg et al. 2009, Jackson et al. 2025).

4.3.2. Role in AMOC variability. Recent observations have revealed a sustained decline in DWBC transport on both sides of Greenland. Koman et al. (2024) documented a 26% drop in DWBC transport denser than $\sigma_0 = 27.8$ kg m^{-3} east of Greenland between 2014 and 2020, which they attributed roughly equally to a thinning of the overflow layer and a weakening of velocities; the layer thinning was caused by freshening of the dense water that deepened the 27.8 kg m^{-3} isopycnal. Using the OSNAP West array on the west side of Greenland, and adopting a lighter density threshold to define the overflow layer, Sun et al. (2025) found a larger reduction of 32% over 2014–2022, with layer thinning dominating over velocity weakening. The layer thinning is consistent with the freshening signal reported by Koman et al. (2024), though the partitioning between thinning and velocity weakening differs, likely reflecting the different density thresholds and locations. Taken together, these results demonstrate that DWBC transport has diminished on both sides of Greenland since 2014.

At the same time, the volume transports of the source waters across the Denmark Strait and Faroe Bank Channel sills have remained stable over this period (Jochumsen et al. 2017, Østerhus et al. 2019, Larsen et al. 2024). Instead, Sun et al. (2025) used a streamtube model (Price & Baringer 1994) to show that decreased downstream entrainment accounts for virtually the entire Denmark Strait Overflow Water (DSOW) transport reduction, and for a substantial fraction of the Northeast Atlantic Deep Water (NEADW) reduction. Warming of the Faroe Bank Channel overflow (Larsen et al. 2024) and freshening of both Denmark Strait and Faroe Bank Channel overflows (Sun et al. 2025) reduced the density contrast between the overflows and the ambient waters above, thereby weakening the entrainment process. These hydrographic changes are consistent with a large-scale freshening anomaly observed across the North Atlantic between 2012 and 2016 that subsequently spread towards the Greenland–Scotland sills (Holliday et al. 2020, Devana et al. 2021). This identifies large-scale subpolar hydrographic variability and accompanying changes in entrainment mixing—rather than overflow sill transport—as the primary control on DWBC transport. This conclusion echoes model studies showing that overflow parameterisations damp AMOC variability by changing density structure rather than through overflow transport directly (Yeager & Danabasoglu 2012).

5. LINKING SUBPOLAR CHANGES WITH SUBTROPICAL OVERTURNING

In the previous section, we examined how water mass transformation, convection, and overflows affect—or fail to affect—the local (subpolar) overturning. The AMOC spans many latitudes, so here we consider how the products of the small-scale diapycnal processes in the subpolar North Atlantic may affect the variability of the subtropical AMOC.

From the RAPID observations at 26°N and several modelling studies (e.g., Frajka-Williams 2015, Polo et al. 2014, 2020) we see that the strongest contributor to $\mathrm{MOC}_z(t)$ at 26°N is $\rho_w(z,t)$ (see also §2.4). This simplification allows us to consider how turbulent pro-

cesses may affect the time variability of the subtropical AMOC. In §3, we showed that much of the seasonal to interannual variability in the subtropical overturning can be explained by local wind forcing, through Ekman transport, through local wind stress curl over the boundary, or through an adjustment to the wind stress curl forcing at the same latitude. From §2.4 and Polo et al. (2014), we expect that to change the thermal wind component of the subtropical and mid-latitude AMOC, the density at the western boundary, weighted towards the depth of maximum overturning, must change.

5.1. Propagation of AMOC signals between latitudes

Changes in subpolar water mass properties must ultimately be communicated to the subtropical Atlantic to affect the overturning at lower latitudes. As discussed in §3, dynamical adjustment through boundary-trapped and basin-crossing waves can propagate signals rapidly—on timescales of 1–10 years—without requiring physical advection of water parcels (Johnson & Marshall 2002, Marshall & Johnson 2013, Pillar et al. 2016, Kostov et al. 2021). Forced ocean models generally show that subpolar AMOC variability is followed by coherent subtropical changes after several years (Bingham et al. 2007, Zhang 2010, Yeager & Danabasoglu 2014), though coupled models exhibit a broader range of coherence depending on timescale and model physics (Xu et al. 2019). Variability in the lower NADW layer (3000–5000 m) forms a key link between the subpolar gyre and subtropical AMOC (Zou et al. 2019). Idealised model studies suggest that the meridional communication of AMOC signals is mediated by rapidly propagating boundary waves at the western boundary of the Atlantic (see **Figure 3**; Johnson & Marshall 2002, Marshall & Johnson 2013, Johnson et al. 2019). Boundary density may provide an additional link between subpolar buoyancy forcing and subtropical AMOC strength (Polo et al. 2014, 2020), consistent with the thermal wind arguments derived in §2.4.

Identifying signals of meridional connectivity in observational data presents considerable challenges. The relatively short records limit the timescales that can be considered (annual to interannual) for direct coherence of transport variability. On subannual timescales, moored observations indicate rapid basin-scale adjustment to wind forcing through barotropic and baroclinic wave processes (Elipot et al. 2016). On interannual timescales, density-based transport estimates compared between 47°N and 26°N (Wett et al. 2023) and between 26°N and 16°N (Frajka-Williams et al. 2018) hint at relatively rapid adjustment (about one year from 47°N to 26°N, and less than 1 year from 26°N to 16°N), though the records are short and the number of degrees of freedom is small. On longer timescales, hydrographic sections reveal coherent temperature and salinity anomalies on isopycnals (i.e., density-compensated T–S anomalies) that propagate toward the subtropics over several years (van Sebille et al. 2011, Le Bras et al. 2017, Fortin & Lozier 2024, Chomiak et al. 2025). Anomalies on isopycnals, however, do not directly modify density gradients and therefore do not necessarily imply changes in overturning transport. Moored transport records at 26°N are starting to be long enough to consider decadal timescale variability, where the low-frequency geostrophic AMOC variability (here approximated as the total MOC_z minus the surface Ekman transport) covaries with the average deep density anomaly as well as salinity anomalies on deep isopycnals (see **Figure 6**). These changes are consistent with western boundary density driving AMOC changes as discussed in §2.4. However, isopycnal depths also fluctuate, so the changes cannot be unambiguously linked to diabatic rather than adiabatic changes.

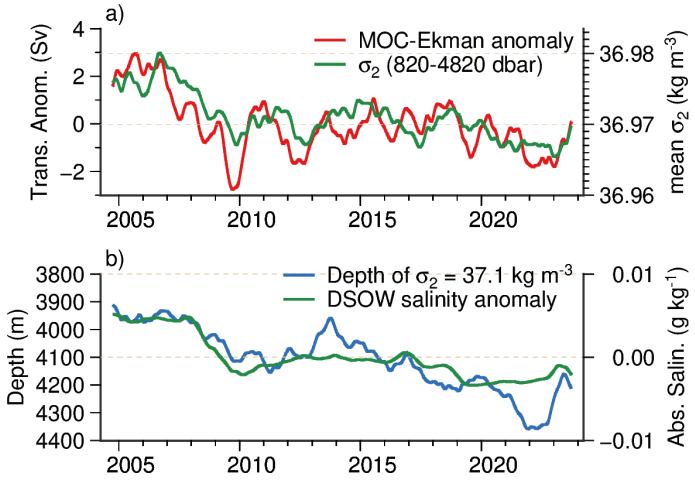


Figure 6

Time series of (a) the MOC-Ekman component of transport and the average σ_2 density in the range 820–4820 dbar near 26.5°N, 76.5°W from the RAPID 26°N array and (b) the depth of the $\sigma_2 = 37.1$ kg m^{-3} isopycnal and absolute salinity anomaly of the waters below this isopycnal, from the same location. Time series have had the seasonal climatology removed and are filtered with a 12-month Tukey filter to focus on the interannual and longer timescales.

Petit et al. (2025) take a different angle on the subpolar–subtropical link, relating mid-latitude overturning strength MOC_z to the density of maximum overturning σ_{moc} in the subpolar region rather than to subpolar overturning strength MOC_σ. A change in σ_{moc} coincides with basin-wide shifts in water mass transformation—towards the production of denser or lighter water masses—which may be communicated rapidly to the subtropics through adiabatic adjustment even when the subpolar overturning strength is unchanged. This shifts the relevant subpolar observable from transport strength (or watermass density) to a property of the overturning circulation itself (the density of maximum overturning), providing an alternate potential link between the turbulent processes discussed in Section 4 and mid-latitude overturning variability; whether σ_{moc} also covaries with proxies of subpolar water-mass transformation (e.g., the density of recently formed Labrador Sea Water) was not evaluated.

Taken together, the studies in this subsection identify several distinct routes by which subpolar conditions can reach the subtropical AMOC: transport-to-transport coherence between latitudes (most clearly seen in forced ocean models), propagation of density anomalies along boundary-trapped wave pathways (which modify the thermal-wind component of subtropical overturning), and—most recently—variations in the density of maximum overturning in the subpolar region that may be communicated through adiabatic adjustment (Petit et al. 2025). Spice anomalies propagating equatorward along isopycnals, while observed in several studies, do not by themselves modify density gradients and so do not directly imply transport changes but may coincide with density changes.

5.2. Boundary vs interior in the subpolar North Atlantic

Overflow waters tend to circulate around the basin boundaries, providing a direct link between overflows and boundary densities. Anomalies generated by deep convection, on the other hand, arise primarily in the interior of subpolar basins. Their influence on large-scale overturning through basin-wide geostrophic transports depends on the signal of change being exported to the basin boundaries where they can modify boundary pressure gradients. This interior-to-boundary communication is a necessary step in the chain linking high-latitude turbulent processes to subtropical AMOC variability.

Interior-to-boundary exchanges have been examined extensively in idealised modelling studies (see review in Johnson et al. 2019). A fundamental result is that regions of deep convection are found in the basin interior while regions of net sinking are localised near the boundaries (Spall & Pickart 2001, Spall 2003), with the downwelling width scaling with the baroclinic deformation radius ($\sim$10 km). Mesoscale eddies play a central role in connecting the two: they transport buoyancy from the boundary current into the convective interior, and return dense convected water to the boundary, allowing downwelling to occur near the boundary even as isopycnals shoal following the mean cyclonic flow (Spall 2010). The temperature, salinity and density of the exported water mass (from interior to boundary) depend on the balance between mean advection along the boundary current, lateral eddy fluxes into the interior, and air–sea buoyancy exchange (Spall 2004, Straneo 2006). Critically, it is the density gradient along the boundaries—not the interior—that controls the strength of the overturning (Spall & Pickart 2001), further supporting our focus on the boundaries in §2.4.

Observational evidence for the export of convective products to the boundary is mixed: Lagrangian pathways to the boundary currents are neither direct nor rapid. Floats deployed during the Labrador Sea deep convection experiment failed to follow the expected pathways into the deep western boundary current to the subtropics (Fischer & Schott 2002). Subsequent Lagrangian studies using isobaric floats or numerical particles found that many trajectories instead followed interior pathways (Bower et al. 2019). However, despite the Lagrangian picture suggesting no rapid connection between the interior and boundary currents, moored array observations show rapid export of interior ventilated waters toward boundary currents (Le Bras et al. 2020, Koelling et al. 2022) with slantwise convection playing a key role (Le Bras et al. 2022). Glider observations in the Labrador Sea find evidence for submesoscale instabilities and strong horizontal gradients that may drive lateral exchange (Clément et al. 2023, 2024). Recent observations in a Southern Hemisphere overflow (Orkney Passage) demonstrate that small-scale, submesoscale processes also occur in deep boundary currents on steep topography (Naveira Garabato et al. 2019), with implications for North Atlantic overflows. These submesoscale processes provide an additional mechanism for boundary-interior exchange in overflow waters that would then modify boundary density.

The recent studies of small-scale processes in the subpolar gyre may help resolve the apparent disconnect between open ocean convection and the generation of density anomalies on the boundary. Once on the boundary, fast wave-adjustment processes can transmit the signal of change to lower latitudes. Quantifying the relative contributions of these pathways to boundary density variability, and establishing the timescales on which they operate, is essential for linking turbulent mixing processes to AMOC variability.

6. DISCUSSION AND OUTLOOK

This review has examined how turbulent processes affect AMOC variability using boundary density as the integrating framework. The thermal wind relation demonstrates that AMOC changes depend on zonal density gradients at basin boundaries, providing a framework for identifying which turbulent processes are dynamically relevant. Adiabatic processes can reposition density surfaces rapidly via boundary waves, while diabatic processes—convection, overflow entrainment, and water mass transformation—irreversibly modify source water properties.

The impacts of these turbulent processes are timescale-dependent. On mean, seasonal and interannual timescales, OSNAP observations show that subpolar AMOC variability is dominated by water mass transformation east of Greenland rather than Labrador Sea convection; model evidence suggests that exceptionally strong forcing in the Labrador Sea can drive multidecadal AMOC changes, a relationship that the current OSNAP record (2014–2022) is too short to resolve (Fu et al. 2025). Overflow entrainment, driven by the density contrast between source and ambient waters, has recently been shown to control DWBC variability despite stable sill flows from the Nordic Seas (Sun et al. 2025). However, despite a 26% decline in DWBC transport east of Greenland since 2014, the AMOC at OSNAP has remained relatively steady over the same period, raising questions about how local DWBC transport relates to subpolar overturning (Koman et al. 2024).

A quantitative link between decadal variability in open ocean convection in the Labrador and Irminger Seas and AMOC variability at lower latitudes remains to be established. Whether the rate-limiting step is the density of the recently formed water masses, the transmission of that density signal to the boundary, or its subsequent propagation equatorward along the western boundary remains unclear. The sensitivity of subtropical and midlatitude AMOC variability to how and where density anomalies appear on the boundary—and whether the resulting signals are large enough to be detectable—is a key open question. The interior-to-boundary pathways that link small-scale turbulent processes to basin-scale changes are not yet well constrained, though recent observations suggest active exchange at mid-depths (Le Bras et al. 2020, 2022). Addressing these questions will require the continued operation of the OSNAP and RAPID arrays, together with targeted boundary observations, to connect subpolar sources of variability to subtropical overturning.

SUMMARY POINTS

1. The geostrophic-shear component of AMOC strength is set by the trans-basin boundary density difference via thermal wind, with a depth-dependent weighting that peaks at the depth of maximum overturning (z_{moc}) and vanishes at the surface and seabed.
2. Both adiabatic and diabatic processes can contribute to AMOC variability, including on short timescales.
3. The subpolar AMOC is set by water mass transformation east of Greenland in the mean and on annual to interannual timescales.
4. Observational evidence linking Labrador Sea convection to subpolar AMOC variability remains inconclusive over the current record, though modelling studies suggest a role on decadal and longer timescales.
5. Since 2014, the deep western boundary current (DWBC) transport has declined

on both sides of Greenland while Nordic Seas overflow transports and the AMOC at OSNAP have remained relatively steady; the DWBC decline is attributable to changes in entrainment downstream of the sills.

FUTURE ISSUES

1. Identifying useful predictors for subtropical AMOC variability (e.g., the subpolar density of maximum overturning or density of Labrador Sea Water) requires testing across longer model integrations and observational records.
2. Improving overflow representation in climate models requires both better parameterisations and reduced biases in the source water properties and surface buoyancy fluxes that drive entrainment.
3. The mechanisms by which interior density anomalies generated by convection and overflows are communicated to the basin boundaries—and their quantitative contribution to boundary density variability—remain poorly constrained by observations.
4. Sustained observations of the AMOC in the subpolar North Atlantic (e.g., the OSNAP array) are needed to determine observationally whether Labrador Sea convection drives AMOC variability—a relationship suggested by modelling studies but not yet resolvable from the current observational record.
5. Continued monitoring of the DWBC on both sides of Greenland, paired with subtropical AMOC observations, is required to establish whether the recent entrainment-driven decline in lower NADW transport continues and whether the resulting density anomalies reach and influence subtropical overturning.

Disclosure Statement

The author is not aware of any affiliations, memberships, funding, or financial holdings that might be perceived as affecting the objectivity of this review.

Acknowledgements

EFW thanks Nicholas Foukal, Gokhan Danabasoglu, and Alberto Naveira Garabato for helpful discussions that shaped the ideas in this paper. Data from the RAPID-MOC-WBTS monitoring project are funded by the Natural Environment Research Council, the National Science Foundation (NSF) with support from NOAA. They are freely available from `https://www.rapid.ac.uk/`. OSNAP data were collected and made freely available by the OSNAP (Overturning in the Subpolar North Atlantic Program) project and all the national programs that contribute to it (`https://www.o-snap.org`). EFW acknowledges funding from the TERIFIC "Targeted Experiment to Reconcile Increased Freshwater with Increased Convection" and EPOC "Explaining and Predicting the Ocean Conveyor" projects funded by the European Union. Views and opinions expressed are however those of the author only and do not necessarily reflect those of the European Union. Neither the European Union nor the granting authority can be held responsible for them.

LITERATURE CITED

Andres M, Yang J, Kwon YO. 2012. Adjustment of a wind-driven two-layer system with mid-basin topography. *Journal of Marine Research* 70(6):851–882

Baringer MO, Price JF. 1997. Mixing and spreading of the Mediterranean Outflow. *Journal of Physical Oceanography* 27(8):1654–1677

Bingham RJ, Hughes CW, Roussenov V, Williams RG. 2007. Meridional coherence of the North Atlantic meridional overturning circulation. *Geophysical Research Letters* 34(23):L23606

Böning CW, Scheinert M, Dengg J, Biastoch A, Funk A. 2006. Decadal variability of subpolar gyre transport and its reverberation in the North Atlantic overturning. *Geophysical Research Letters* 33(21):L21S01

Böning CW, Wagner P, Handmann P, Schwarzkopf FU, Getzlaff K, Biastoch A. 2023. Decadal changes in Atlantic overturning due to the excessive 1990s Labrador Sea convection. *Nature Communications* 14(1):4635

Bower AS, Lozier MS, Biastoch A, Drouin K, Foukal N, et al. 2019. Lagrangian views of the pathways of the Atlantic meridional overturning circulation. *Journal of Geophysical Research* 124:5313–5335

Buckley MW, Lozier MS, Desbruyères D, Evans DG. 2023. Buoyancy forcing and the subpolar Atlantic meridional overturning circulation. *Phil. Trans. R. Soc. A* 381:20220181

Buckley MW, Marshall J. 2016. Observations, inferences, and mechanisms of the Atlantic meridional overturning circulation: A review. *Reviews of Geophysics* 54(1):1–59

Chidichimo MP, Kanzow T, Cunningham SA, Johns WE, Marotzke J. 2010. The contribution of eastern-boundary density variations to the Atlantic meridional overturning circulation at 26.5°N. *Ocean Science* 6(2):475–490

Chomiak LN, Volkov DL, Johns WE, V JAH, Smith RH. 2025. Deep ocean cooling and freshening from subpolar North Atlantic reaches subtropics at 26.5°N. *Communications Earth & Environment* 6(1):235

Cimoli L, et al. 2023. Significance of diapycnal mixing within the Atlantic meridional overturning circulation. *AGU Advances* 4(2):e2022AV000800

Clément L, Frajka-Williams E, von Oppeln-Bronikowski N, Goszczko I, de Young B. 2023. Cessation of Labrador Sea convection triggered by distinct fresh and warm (sub)mesoscale flows. *Journal of Physical Oceanography* 53(8):1959–1977

Clément L, Merckelbach L, Frajka-Williams E. 2024. Turbulent vertical velocities in Labrador Sea convection. *Geophysical Research Letters* 51(21):e2024GL110318

Danabasoglu G, Castruccio FS, Boza B, Barthel AM, Biastoch A, et al. 2025. Simulated and observed transport estimates across the Overturning in the Subpolar North Atlantic Program (OSNAP) section. *EGUsphere* 2025:1–89

Danabasoglu G, Large WG, Briegleb BP. 2010. Climate impacts of parameterized Nordic Sea overflows. *Journal of Geophysical Research: Oceans* 115(C11):C11005

Danabasoglu G, Yeager SG, Bailey D, Behrens E, Bentsen M, et al. 2014. North Atlantic simulations in Coordinated Ocean-ice Reference Experiments phase II (CORE-II). Part I: Mean states. *Ocean Modelling* 73:76–107

de Lavergne C, Groeskamp S, Zika J, Johnson HL. 2021. The role of mixing in the large-scale ocean circulation. In *Ocean Mixing: Drivers, mechanisms and impacts*, eds. M Meredith, A Naveira Garabato. Oxford, United Kingdom: Elsevier, 35–64

Desbruyères DG, Mercier H, Maze G, Daniault N. 2019. Surface predictor of overturning circulation and heat content change in the subpolar North Atlantic. *Ocean Science* 15(3):809–817

Devana MS, Johns WE, Houk A, Zou S. 2021. Rapid freshening of Iceland Scotland Overflow Water driven by entrainment of a major upper ocean salinity anomaly. *Geophysical Research Letters* 48:e2021GL094396

Dickson RR, Brown J. 1994. The production of North Atlantic Deep Water: Sources, rates, and pathways. *Journal of Geophysical Research: Oceans* 99(C6):12319–12341

Duchez A, Frajka-Williams E, Castro N, Hirschi J, Coward A. 2014a. Seasonal to interannual variability in density around the Canary Islands and their influence on the Atlantic meridional overturning circulation at 26°N. *Journal of Geophysical Research: Oceans* 119(3):1843–1860

Duchez A, Hirschi JJM, Cunningham SA, Blaker AT, Bryden HL, et al. 2014b. A new index for the Atlantic meridional overturning circulation at 26°N. *Journal of Climate* 27(17):6439–6455

Elipot S, Frajka-Williams E, Hughes CW, Olhede S, Lankhorst M. 2016. Observed basin-scale response of the North Atlantic meridional overturning circulation to wind stress forcing. *Journal of Climate* 30(6):2029–2054

Evans DG, Holliday NP, Bacon S, Bras IL. 2023. Mixing and air–sea buoyancy fluxes set the time-mean overturning circulation in the subpolar North Atlantic and Nordic Seas. *Ocean Science* 19(3):745–768

Evans DG, Toole J, Forget G, Zika JD, Naveira Garabato AC, et al. 2017. Recent wind-driven variability in Atlantic water mass distribution and meridional overturning circulation. *Journal of Physical Oceanography* 47(3):633–647

Fischer J, Schott FA. 2002. Labrador Sea Water tracked by profiling floats—From the boundary current into the open North Atlantic. *Journal of Physical Oceanography* 32(2):573–584

Fortin A, Lozier MS. 2024. Competition between advected and local variability determines coherent propagation of Labrador Sea Water along the DWBC. *Journal of Geophysical Research: Oceans* 129(12):e2024JC021241

Foukal N, Chafik L. 2024. Consensus around a common definition of Atlantic Overturning will promote progress. *Oceanography* 37(3):10–15

Fox AD, Fraser NJ, Burmeister K, Jones SC, Cunningham SA, et al. 2026. The Scotland-Canada overturning array (SCOTIA): Twenty years of meridional overturning in the subpolar North Atlantic. *Ocean Science* 22:1439–1456

Frajka-Williams E, Ansorge IJ, Baehr J, Bryden HL, Chidichimo MP, et al. 2019. Atlantic meridional overturning circulation: Observed transport and variability. *Frontiers in Marine Science* 6:260

Frajka-Williams E, Bamber J, Våge K. 2016a. Greenland melt and the Atlantic meridional overturning circulation. *Oceanography* 29(4):22–33

Frajka-Williams E, Eriksen CC, Rhines PB, Harcourt RR. 2011. Determining vertical water velocities from Seaglider. *Journal of Atmospheric and Oceanic Technology* 28(12):1641–1656

Frajka-Williams E, Foukal N, Danabasoglu G. 2023. Should AMOC observations continue: How and why? *Philosophical Transactions of the Royal Society A* 381(2262):20220195

Frajka-Williams E, Meinen CS, Johns WE, Smeed DA, Duchez A, et al. 2016b. Compensation between meridional flow components of the Atlantic MOC at 26°N. *Ocean Science* 12(2):481–493

Frajka-Williams E. 2015. Estimating the Atlantic overturning at 26°N using satellite altimetry and cable measurements. *Geophysical Research Letters* 42(9):3458–3464

Frajka-Williams E, Lankhorst M, Koelling J, Send U. 2018. Coherent circulation changes in the deep North Atlantic from 16°N and 26°N transport arrays. *Journal of Geophysical Research: Oceans* 123(5):3427–3443

Fu Y, Lozier MS, Bower A, Burmeister K, Biló TC, et al. 2025. Characterizing the interannual variability of North Atlantic subpolar overturning. *Geophysical Research Letters* 52(19):e2025GL114672

Good SA, Martin MJ, Rayner NA. 2013. En4: quality controlled ocean temperature and salinity profiles and monthly objective analyses with uncertainty estimates. *Journal of Geophysical Research: Oceans* 118:6704–6716

Groeskamp S, Griffies SM, Iudicone D, Marsh R, Nurser AG, Zika JD. 2018. The water mass transformation framework for ocean physics and biogeochemistry. *Annual Review of Marine Science* 11(1):271–305

Heuzé C. 2021. Antarctic Bottom Water and North Atlantic Deep Water in CMIP6 models. *Ocean Science* 17(1):59–90

Holliday NP, Bersch M, Berx B, Chafik L, Cunningham S, et al. 2020. Ocean circulation causes the

largest freshening event for 120 years in eastern subpolar North Atlantic. *Nature Communications* 11(1):585

Hughes CW, Elipot S, Maqueda MÁM, Loder JW. 2013. Test of a method for monitoring the geostrophic meridional overturning circulation using only boundary measurements. *Journal of Atmospheric and Oceanic Technology* 30(4):789–809

Hughes CW, Williams J, Blaker A, Coward A, Stepanov V. 2018. A window on the deep ocean: The special value of ocean bottom pressure for monitoring the large-scale, deep-ocean circulation. *Progress in Oceanography* 161:19–46

Hughes G, Griffiths R. 2006. A simple convective model of the global overturning circulation, including effects of entrainment into sinking regions. *Ocean Modelling* 12:46–79

Jackson LC, Biastoch A, Buckley MW, Desbruyères DG, Frajka-Williams E, et al. 2022. The evolution of the North Atlantic meridional overturning circulation since 1980. *Nature Reviews Earth & Environment* 3(4):241–254

Jackson LC, Chassignet EP, Danabasoglu G, Treguier A, Zhang R. 2025. Toward improving representation of the Atlantic meridional overturning circulation in climate models. *Bulletin of the American Meteorological Society* 106(6):E1032–E1036

Jackson LC, Peterson KA, Roberts CD, Wood RA. 2016. Recent slowing of Atlantic overturning circulation as a recovery from earlier strengthening. *Nature Geoscience* 9(7):518–522

Jochumsen K, Moritz M, Nunes N, Quadfasel D, Larsen KMH, et al. 2017. Revised transport estimates of the Denmark Strait overflow. *Journal of Geophysical Research: Oceans* 122(4):3434–3450

Johns WE, Beal LM, Baringer MO, Molina JR, Cunningham SA, et al. 2008. Variability of shallow and deep western boundary currents off the Bahamas during 2004–05: Results from the 26°N RAPID–MOC Array. *Journal of Physical Oceanography* 38(3):605–623

Johnson HL, Cessi P, Marshall DP, Schloesser F, Spall MA. 2019. Recent contributions of theory to our understanding of the Atlantic meridional overturning circulation. *Journal of Geophysical Research: Oceans* 124(8):5376–5399

Johnson HL, Marshall DP. 2002. A theory for the surface Atlantic response to thermohaline variability. *Journal of Physical Oceanography* 32(4):1121–1132

Kanzow T, Cunningham SA, Johns WE, Hirschi JJM, Marotzke J, et al. 2010. Seasonal variability of the Atlantic meridional overturning circulation at 26.5°N. *Journal of Climate* 23(21):5678–5698

Kanzow T, Cunningham SA, Rayner D, Hirschi JJM, Johns WE, et al. 2007. Observed flow compensation associated with the MOC at 26.5°N in the Atlantic. *Science* 317(5840):938–941

Koelling J, Atamanchuk D, Karstensen J, Handmann P, Wallace DWR. 2022. Oxygen export to the deep ocean following Labrador Sea Water formation. *Biogeosciences* 19:437–454

Koman G, Bower AS, Holliday NP, Furey HH, Fu Y, Biló TC. 2024. Observed decrease in Deep Western Boundary Current transport in subpolar North Atlantic. *Nature Geoscience* 17(11):1148–1153

Kostov Y, Johnson HL, Marshall DP, Heimbach P, Forget G, et al. 2021. Distinct sources of interannual subtropical and subpolar Atlantic overturning variability. *Nature Geoscience* 14(7):491–495

Kuhlbrodt T, Griesel A, Montoya M, Levermann A, Hofmann M, Rahmstorf S. 2007. On the driving processes of the Atlantic meridional overturning circulation. *Reviews of Geophysics* 45(2)

Larsen KMH, Hansen B, Hátún H, Johansen GE, Østerhus S, Olsen SM. 2024. The coldest and densest overflow branch into the North Atlantic is stable in transport, but warming. *Geophysical Research Letters* 51(16):e2024GL110097

Le Bras IA, Callies J, Straneo F, Biló TC, Holte J, Johnson HL. 2022. Slantwise convection in the Irminger Sea. *Journal of Geophysical Research: Oceans* 127(10):e2022JC019071

Le Bras IA, Straneo F, Holte J, Jong MF, Holliday NP. 2020. Rapid export of waters formed by convection near the Irminger Sea's western boundary. *Geophysical Research Letters* 47(3):e2019GL085989

Le Bras IA, Yashayaev I, Toole JM. 2017. Tracking Labrador Sea Water property signals along the Deep Western Boundary Current. *Journal of Geophysical Research: Oceans* 122:5348–5366

Legg S, Ezer T, Jackson L, Briegleb B, Danabasoglu G, et al. 2009. Improving oceanic overflow representation in climate models: The Gravity Current Entrainment Climate Process Team. *Bulletin of the American Meteorological Society* 90(5):657–670

Legg S, Hallberg RW, Girton JB. 2006. Comparison of entrainment in overflows simulated by z-coordinate, isopycnal and non-hydrostatic models. *Ocean Modelling* 11(1):69–97

Lherminier P, Mercier H, Gourcuff C, Alvarez M, Bacon S, Kermabon C. 2007. Transports across the 2002 Greenland-Portugal Ovide section and comparison with 1997. *Journal of Geophysical Research: Oceans* 112(C7):C07003

Li F, Lozier MS. 2018. On the linkage between Labrador Sea Water volume and overturning circulation in the Labrador Sea: A case study on proxies. *Journal of Climate* 31(13):5225–5241

Li F, Lozier MS, Danabasoglu G, Holliday NP, Kwon YO, et al. 2019. Local and downstream relationships between Labrador Sea Water volume and North Atlantic meridional overturning circulation variability. *Journal of Climate* 32(13):3883–3898

Li F, Lozier MS, Johns WE. 2017. Calculating the meridional volume, heat, and freshwater transports from an observing system in the subpolar North Atlantic: Observing System Simulation Experiment. *Journal of Atmospheric and Oceanic Technology* 34(7):1483–1500

Lozier MS. 2012. Overturning in the North Atlantic. *Annual Review of Marine Science* 4(1):291–315

Lozier MS, Li F, Bacon S, Bahr F, Bower AS, et al. 2019. A sea change in our view of overturning in the subpolar North Atlantic. *Science* 363(6426):516–521

Marotzke J, Giering R, Zhang KQ, Stammer D, Hill C, Lee T. 1999. Construction of the adjoint MIT ocean general circulation model and application to Atlantic heat transport sensitivity. *Journal of Geophysical Research: Oceans* 104(C12):29529–29547

Marshall DP, Johnson HL. 2013. Propagation of meridional circulation anomalies along western and eastern boundaries. *Journal of Physical Oceanography* 43(12):2699–2717

Marshall J, Schott F. 1999. Open-ocean convection: Observations, theory and models. *Reviews of Geophysics* 37(1):1–64

McCarthy G, Frajka-Williams E, Johns WE, Baringer MO, Meinen CS, et al. 2012. Observed interannual variability of the Atlantic meridional overturning circulation at 26.5°N. *Geophysical Research Letters* 39(19):L19609

McCarthy G, Smeed D, Johns W, Frajka-Williams E, Moat B, et al. 2015. Measuring the Atlantic meridional overturning circulation at 26°N. *Progress in Oceanography* 130:91–111

Menary MB, Jackson LC, Lozier MS. 2020. Reconciling the relationship between the AMOC and Labrador Sea in OSNAP observations and climate models. *Geophysical Research Letters* 47(18):e2020GL089793

Moat BI, Smeed DA, Frajka-Williams E, Desbruyères DG, Beaulieu C, et al. 2020. Pending recovery in the strength of the meridional overturning circulation at 26°N. *Ocean Science* 16(4):863–874

Moat BI, Smeed DA, Rayner D, Johns WE, Smith R, et al. 2026. Atlantic meridional overturning circulation observed by the RAPID-MOCHA-WBTS (RAPID-Meridional Overturning Circulation and Heatflux Array-Western Boundary Time Series) array at 26°N from 2004 to 2024 (v2024.1a)

Munk WH. 1966. Abyssal recipes. *Deep Sea Research* 13:707–730

Naveira Garabato AC, Frajka-Williams EE, Spingys CP, Legg S, Polzin KL, et al. 2019. Rapid mixing and exchange of deep-ocean waters in an abyssal boundary current. *Proceedings of the National Academy of Sciences* 116(27):13233–13238

Østerhus S, Woodgate R, Valdimarsson H, Turrell B, Steur Ld, et al. 2019. Arctic Mediterranean exchanges: A consistent volume budget and trends in transports from two decades of observations. *Ocean Science* 15(2):379–399

Petit T, Robson J, Ferreira D, Yeager S, Evans DG. 2025. Coherence of the AMOC over the subpolar North Atlantic on interannual to multiannual time scales. *Geophysical Research Letters* 52(9):e2025GL115171

Pickart RS, Spall MA. 2007. Impact of Labrador Sea convection on the North Atlantic meridional overturning circulation. *Journal of Physical Oceanography* 37(9):2207–2227

Pillar HR, Heimbach P, Johnson HL, Marshall DP. 2016. Dynamical attribution of recent variability in Atlantic overturning. *Journal of Climate* 29(9):3339–3352

Polo I, Haines K, Robson J, Thomas C. 2020. Can the boundary profiles at 26°N be used to extract buoyancy-forced Atlantic meridional overturning circulation signals? *Ocean Science* 16(5):1067–1088

Polo I, Robson J, Sutton R, Balmaseda MA. 2014. The importance of wind and buoyancy forcing for the boundary density variations and the geostrophic component of the AMOC at 26°N. *Journal of Physical Oceanography* 44(9):2387–2408

Price JF, Baringer MO. 1994. Outflows and deep water production by marginal seas. *Progress in Oceanography* 33(3):161–200

Richardson PL. 2008. On the history of meridional overturning circulation schematic diagrams. *Progress in Oceanography* 76(4):466–486

Robson J, Hodson D, Hawkins E, Sutton R. 2014. Atlantic overturning in decline? *Nature Geoscience* 7(1):2–3

Schiller-Weiss I, Martin T, Schwarzkopf FU. 2024. Emerging influence of enhanced Greenland melting on boundary currents and deep convection regimes in the Labrador and Irminger Seas. *Geophysical Research Letters* 51(9):e2024GL109022

Sinha B, Smeed D, McCarthy G, Moat B, Josey S, et al. 2018. The accuracy of estimates of the overturning circulation from basin-wide mooring arrays. *Progress in Oceanography* 160:101–123

Spall MA. 2003. On the thermohaline circulation in flat bottom marginal seas. *Journal of Marine Research* 61:1–25

Spall MA. 2004. Boundary currents and watermass transformation in marginal seas. *Journal of Physical Oceanography* 34(6):1197–1213

Spall MA. 2010. Dynamics of downwelling in an eddy-resolving convective basin. *Journal of Physical Oceanography* 40(10):2341–2347

Spall MA, Pickart RS. 2001. Where does dense water sink? A subpolar gyre example*. *Journal of Physical Oceanography* 31(3):810–826

Steffen EL, D'Asaro EA. 2002. Deep convection in the Labrador Sea as observed by Lagrangian floats. *Journal of Physical Oceanography* 32(2):475–492

Straneo F. 2006. On the connection between dense water formation, overturning, and poleward heat transport in a convective basin*. *Journal of Physical Oceanography* 36(9):1822–1840

Sun Y, Pickart RS, Lin P, Pacini A, Macrander A, et al. 2025. Reduced transport of overflow water in the West Greenland boundary current system: The role of upstream entrainment. *Journal of Physical Oceanography* 55(11):2119–2139

Tooth OJ, Foukal NP, Johns WE, Johnson HL, Wilson C. 2024. Lagrangian decomposition of the Atlantic Ocean heat transport at 26.5°N. *Geophysical Research Letters* 51(14)

van Sebille E, Baringer MO, Johns WE, Meinen CS, Beal LM, et al. 2011. Propagation pathways of classical Labrador Sea water from its source region to 26°N. *Journal of Geophysical Research: Oceans* 116(C12):C12027

Voet G, Quadfasel D. 2010. Entrainment in the Denmark Strait overflow plume by meso-scale eddies. *Ocean Science* 6(1):301–310

Waldman R, Hirschi J, Voldoire A, Cassou C, Msadek R. 2021. Clarifying the relation between AMOC and thermal wind: Application to the centennial variability in a coupled climate model. *Journal of Physical Oceanography* 51(2):343–364

Walin G. 1982. On the relation between sea-surface heat flow and thermal circulation in the ocean. *Tellus* 34(2):187–195

Wang H, Legg SA, Hallberg RW. 2015. Representations of the Nordic Seas overflows and their large scale climate impact in coupled models. *Ocean Modelling* 86:76–92

Wett S, Rhein M, Kieke D, Mertens C, Moritz M. 2023. Meridional connectivity of a 25-year observational AMOC record at 47°N. *Geophysical Research Letters* 50(16):e2023GL103284

Worthington EL, Frajka-Williams E, McCarthy GD. 2019. Estimating the deep overturning trans-

port variability at 26°N using bottom pressure recorders. *Journal of Geophysical Research: Oceans* 124(1):335–348

Xing Q, Elipot S, Johns WE, Smeed DA, Moat BI, Loder JW. 2026. Meridionally-consistent decline in the observed western boundary contribution to the Atlantic meridional overturning circulation. *Science Advances*

Xu X, Chassignet EP, Wang F. 2019. On the variability of the Atlantic meridional overturning circulation transports in coupled CMIP5 simulations. *Climate Dynamics* 52(11):6511–6531

Yeager S, Castruccio F, Chang P, Danabasoglu G, Maroon E, et al. 2021. An outsized role for the Labrador Sea in the multidecadal variability of the Atlantic overturning circulation. *Science Advances* 7(41):eabh3592

Yeager S, Danabasoglu G. 2012. Sensitivity of Atlantic meridional overturning circulation variability to parameterized Nordic Sea overflows in CCSM4. *Journal of Climate* 25(6):2077–2103

Yeager S, Danabasoglu G. 2014. The origins of late-twentieth-century variations in the large-scale North Atlantic circulation. *Journal of Climate* 27:3222–3247

Zhang R. 2010. Latitudinal dependence of Atlantic meridional overturning circulation (AMOC) variations. *Geophysical Research Letters* 37(16):L16703

Zhang R, Sutton R, Danabasoglu G, Kwon Y, Marsh R, et al. 2019. A review of the role of the Atlantic meridional overturning circulation in Atlantic Multidecadal Variability and associated climate impacts. *Reviews of Geophysics* 57(2):316–375

Zhang R, Thomas M. 2021. Horizontal circulation across density surfaces contributes substantially to the long-term mean northern Atlantic meridional overturning circulation. *Communications Earth & Environment* 2(1):112

Zhao J, Johns W. 2014a. Wind-driven seasonal cycle of the Atlantic meridional overturning circulation. *Journal of Physical Oceanography* 44(6):1541–1562

Zhao J, Johns W. 2014b. Wind-forced interannual variability of the Atlantic meridional overturning circulation at 26.5°N. *Journal of Geophysical Research: Oceans* 119(4):2403–2419

Zou S, Lozier MS. 2016. Breaking the linkage between Labrador Sea Water production and its advective export to the subtropical gyre. *Journal of Physical Oceanography* 46(7):2169–2182

Zou S, Lozier MS, Buckley M. 2019. How is meridional coherence maintained in the lower limb of the Atlantic meridional overturning circulation? *Geophysical Research Letters* 46(1):244–252